Supporting Information

Fluorinated COF-Encapsulated CeO_2@Pt Sandwich Catalyst Enables Dual Interfacial-Electronic Modulation for Liquid-Phase Hydrogenation

Rongyao Wang[a, b#], Peiao Cong[a#], Shuai Wang[a], Luqing Zhang[a]*, Daowei Gao[a], Guozhu Chen[a*]

a School of Chemistry and Chemical Engineering, University of Jinan, Jinan, Shandong Province, 250022 P.R. China.

b School of Water Conservancy and Environment, University of Jinan, Jinan, 250022, Province, 250022 P.R. China.

[#] Rongyao Wang and Peiao Cong contributed equally to this work.

*Corresponding authors:

Email: chm_chengz@ujn.edu.cn (Guozhu Chen)

E-mail: chm_zhanglq@ujn.edu.cn (Luqing Zhang)

Text S1 Catalyst synthesis

Synthesis of Pt nanoparticles (Pt NPs). 16.6 mg of PVP was dissolved in 45 mL of ethanol, followed by the dropwise addition of 5.0 mL of H_2PtCl_6 (6.0 mM). After stirring for 2 minutes at room temperature, the mixture was transferred to a three-neck flask with a capacity of 100 mL and heated at 90 ℃ for a duration of 3 h to synthesize Pt nanoparticles stabilized by PVP.

Synthesis of CeO_2. 4 g of $Ce(NO_3)_3 \cdot 6H_2O$, 1.6 g PVP, and 4.2 mL of deionized water were dispersed in 120 mL of ethylene glycol and stirred at room temperature for 30 minutes. The mixture was then heated at 160°C for 8 h, cooled to room temperature, centrifuged at 9800 rpm for 15 min, and purified three times with ultrapure water and absolute ethanol successively. The solid obtained was dried in vacuum and further calcined at 300°C for 1 h in a muffle furnace. Finally, a light yellow CeO_2 powder was obtained.

Text S2. DFT Computational details

All calculations were performed using the spin-polarized density functional theory (DFT) method through Vienna Ab initio Simulation Package (VASP5.4.4) [1,2]. Generalized gradient approximation (GGA) of Perdew-Burke Ernzerhof (PBE) were adopted to describe exchange correlation interaction [3]. The ion-electron interaction was treated using the projector augmented wave (PAW) technique [4]. The plane-wave cutoff energy of 450 eV was employed. The atomic positions were fully relaxed until the maximum force on each atom was less than 0.02 eV/Å. The Brillouin zone was sampled using the Monkhorst-Pack scheme with a k-point mesh of 2×2×1 in the Γ-centered grids for the structural relaxation. Van der Waals interaction was considered using the semiempirical DFT-D3 approach [5]. A vacuum distance of ~15 Å was used to avoid interactions between neighboring layers. A Pt cluster supported on CeO_2(111) was used as the representative model to approximate surface undercoordinated Pt sites. This model captures local charge redistribution trends, while the experimentally observed Pt nanoparticles (~3.3 nm, Fig. S1) provide the realistic size context.

The adsorption energies E_{Ads} of styrene species on various surfaces were calculated using the equation:

$$E_{Ads} = E_{\text{cat-mol}} - E_{\text{cat}} - E_{\text{mol}}$$

Where $E_{\text{cat-mol}}$ is the total energy after adsorption of CeO_2@Pt@TAFA and styrene species, E_{cat} is the energy after optimization of the CeO_2@Pt@TAFA catalyst and E_{mol} is the energy after optimization of styrene species.

Text S3. Molecular dynamics simulations

The molecular dynamics (MD) simulations of CeO_2@Pt@TPA-H_2, CeO_2@Pt@TAFA–H_2, CeO_2@Pt@TPA–styrene, and CeO_2@Pt@TAFA–styrene systems were carried out using the LAMMPS software package. The universal force field (UFF) was employed to describe the COF with full atomistic detail, while the water molecules were modeled using the SPCE force field. A cutoff radius of 10 Å was applied for van der Waals interactions, and long-range electrostatic interactions were treated using the particle–particle particle–mesh (PPPM) method. Each system was first equilibrated under the NPT ensemble at 300 K for 1 ns, followed by a 1 ns equilibration under the NVT ensemble at 1 atm. Subsequently, a 3 ns production run was performed under the NVT ensemble with a time step of 1 fs. The temperature was controlled using the Nosé–Hoover thermostat, while pressure was regulated via the Berendsen barostat. Based on the resulting simulation trajectories, the mean square displacement (MSD) was calculated using the standard expression.

$$MSD(\Delta t) = \left\langle \left| \vec{\Delta r}(\Delta t) \right|^2 \right\rangle = \frac{1}{N} \sum_{i=1}^{N} \left\langle \left| \vec{r}_i(t_i + \Delta t) - \vec{r}_i(t_i) \right|^2 \right\rangle$$

where t denotes time and r(t) represents the position vector of the diffusing molecules. All simulations were conducted under periodic boundary conditions.

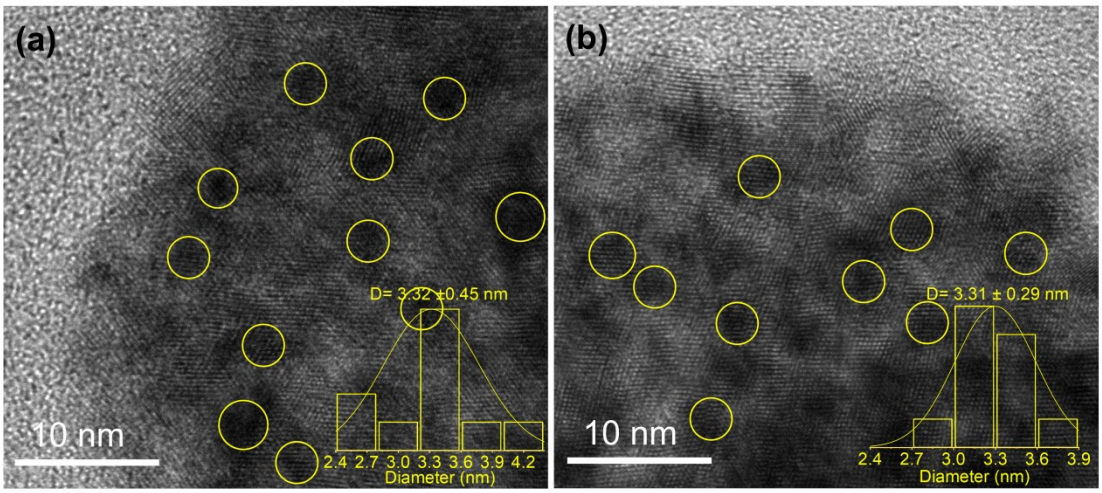

Fig. S1 HRTEM images of (a) CeO_2@Pt@TPA and CeO_2@Pt@TAFA.

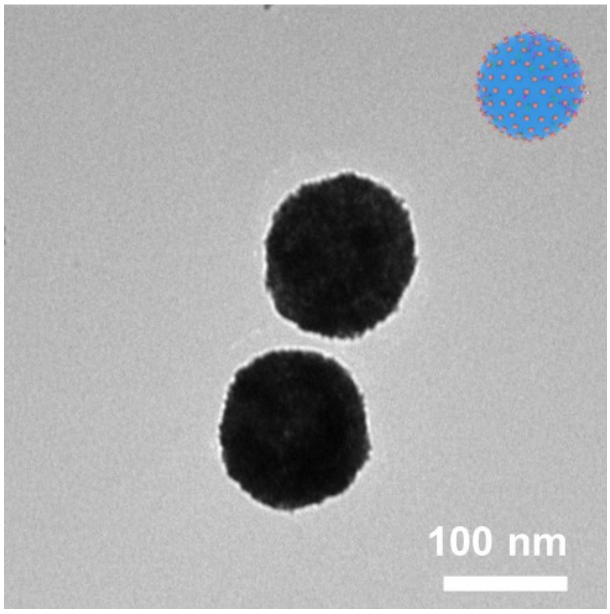

Fig. S2 TEM image of CeO_2@Pt-PB.

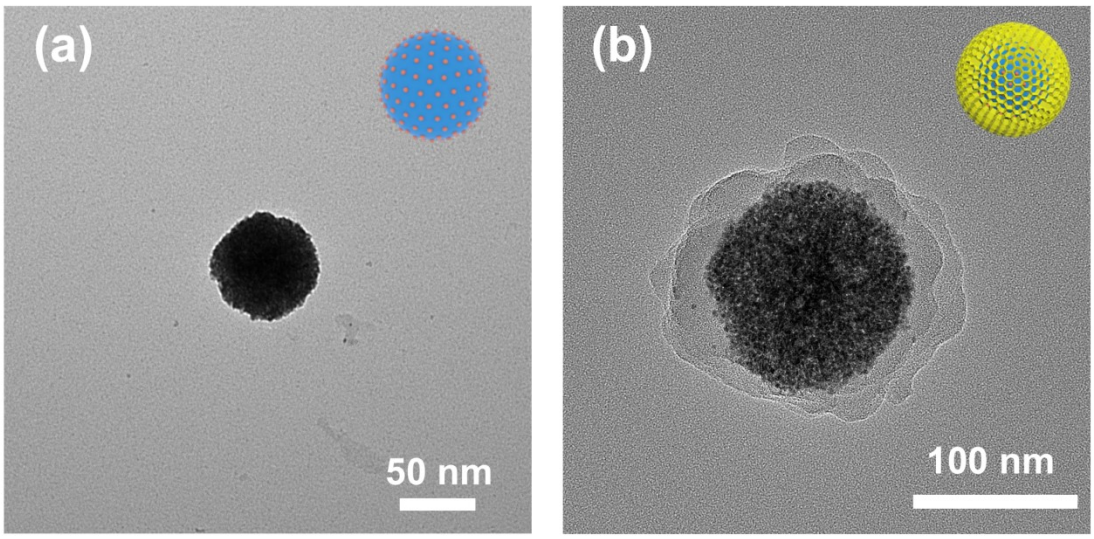

Fig. S3 TEM image of CeO_2@Pt and CeO_2@Pt-TAFA.

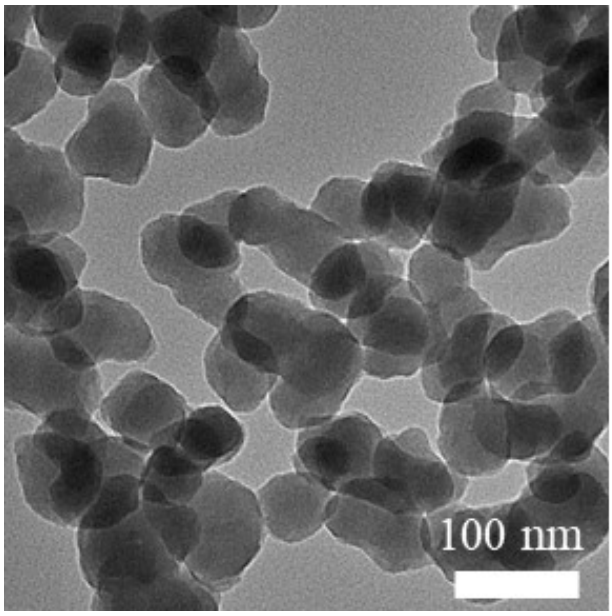

Fig. S4 TEM image of TAFA.

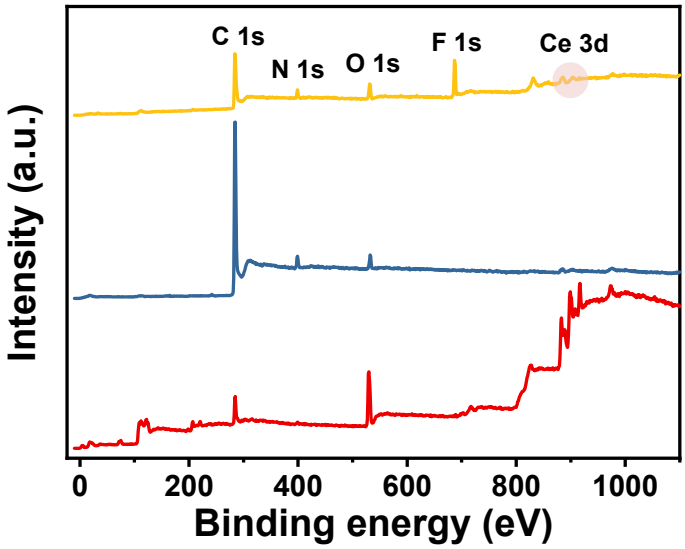

Fig. S5 XPS of CeO_2@Pt, CeO_2@Pt@TPA, and CeO_2@Pt-TAFA.

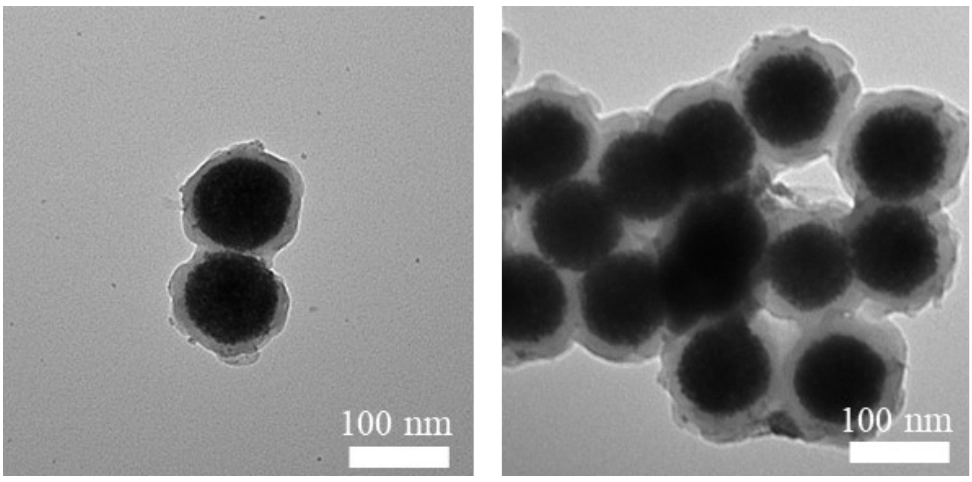

Fig. S6 TEM image of CeO_2@Pt@TAFA after reaction.

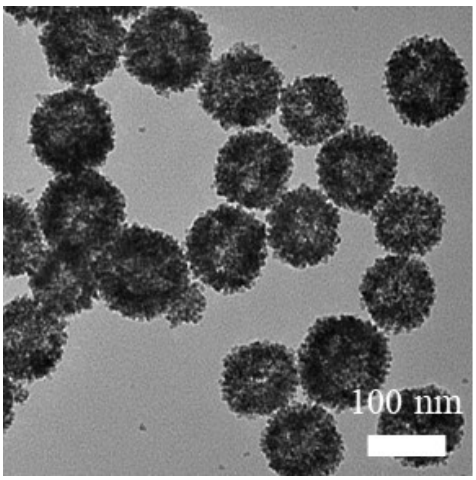

Fig. S7 TEM image of CeO_2@Pt after reaction.

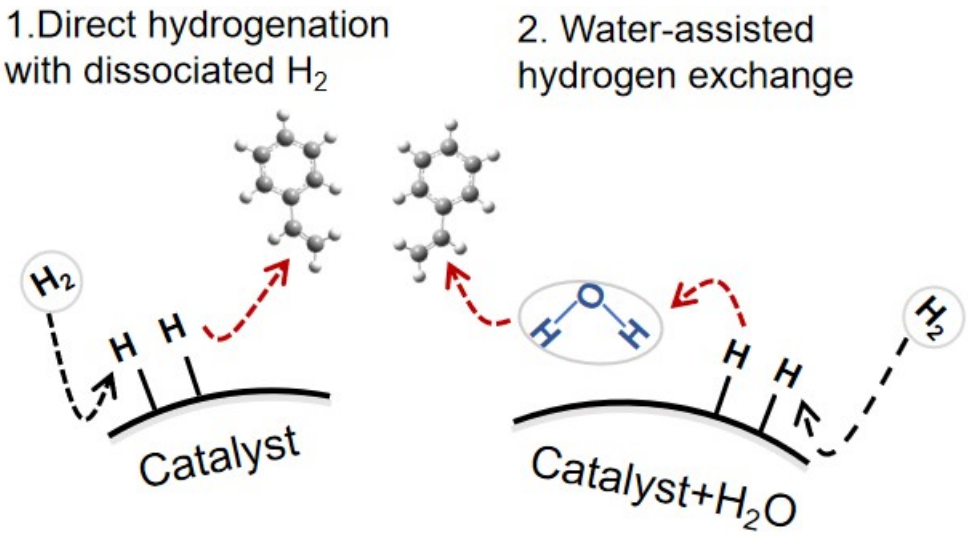

Fig. S8 Schematic illustration of two possible reaction pathways for the hydrogenation process of styrene.

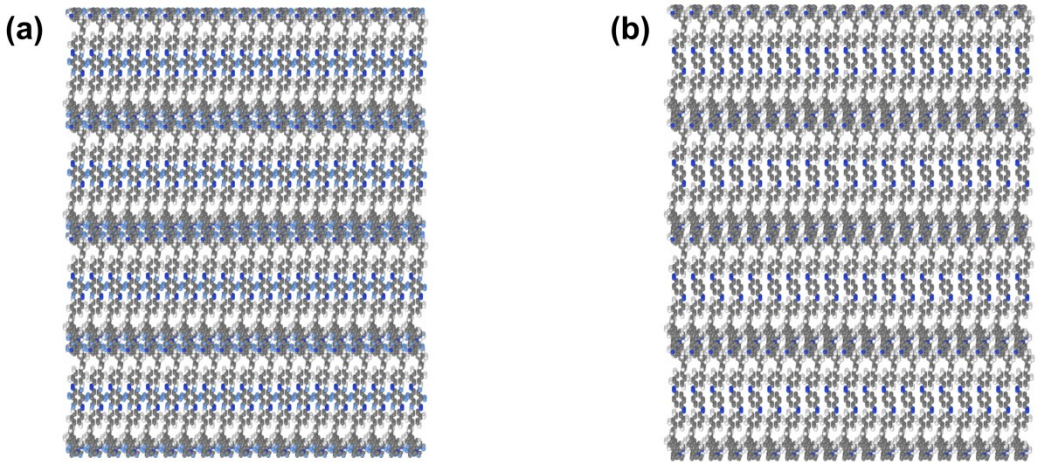

Fig. S9 The structures of (a) TAFA and (b) TPA shells.

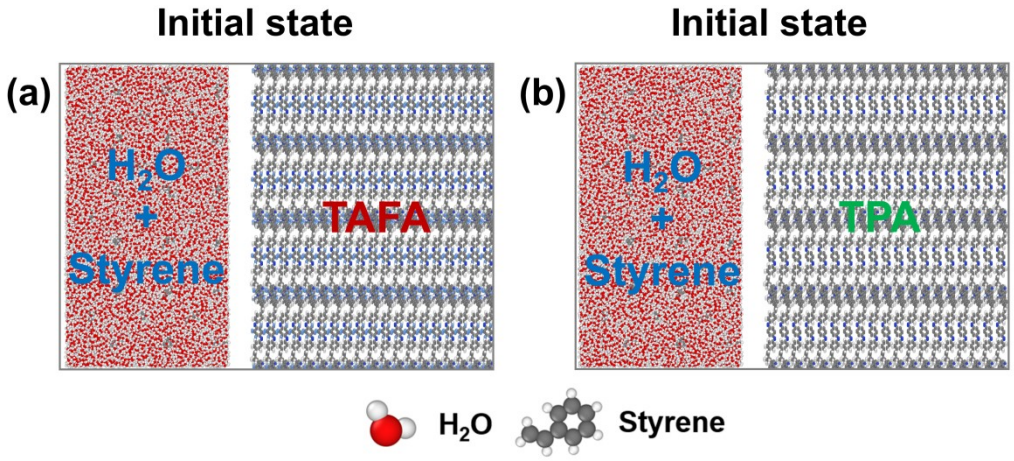

Fig. S10 The snapshot of initial state in the styrene diffusion simulation of (a) TAFA and (b) TPA shells.

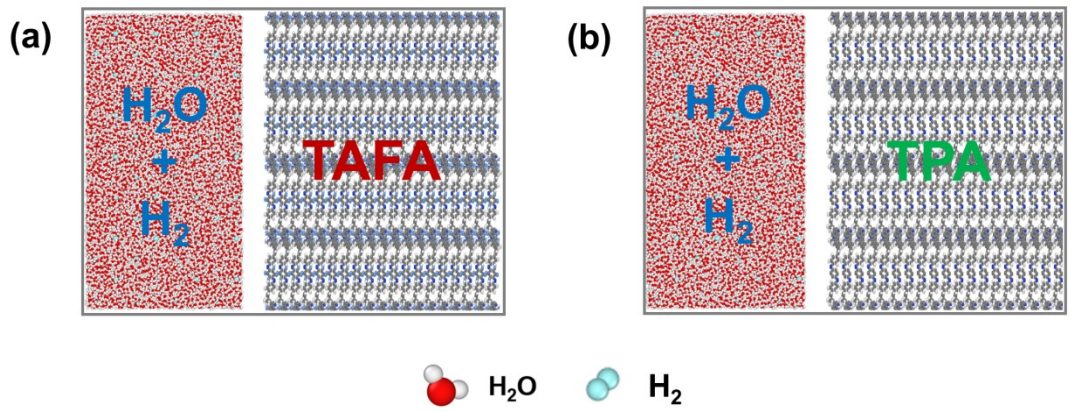

Fig. S11 The snapshot of initial state in the H_2 diffusion simulation of (a) TAFA and (b) TPA shells.

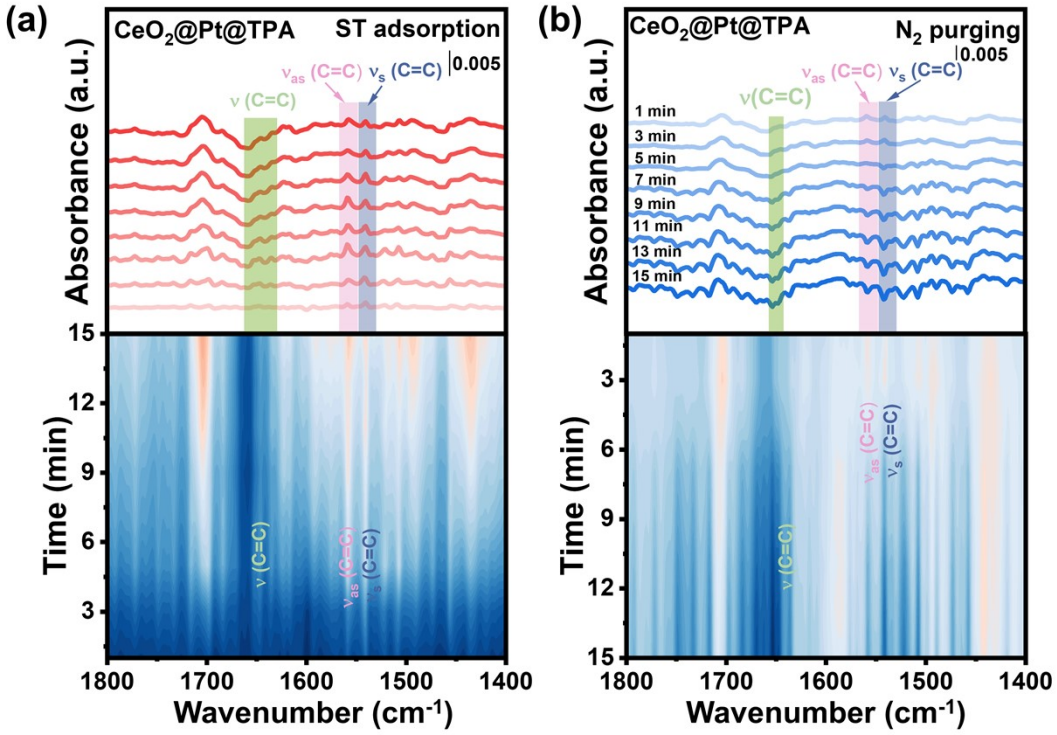

Fig. S12 In situ DRIFTS spectra of (a) styrene adsorption and (b) N_2 purge on CeO_2@Pt@TPA at room temperature.

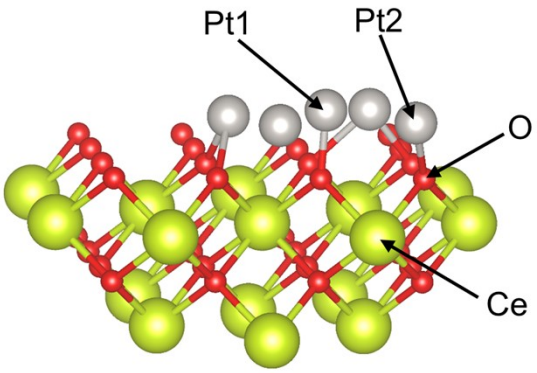

Atom	Pt1	Pt2	O	Ce
Bader (e)	-0.138	-0.411	-0.844	1.86

Fig. S13 An optimized structural model of CeO_2@Pt (top), and calculated Bader charges (bottom).

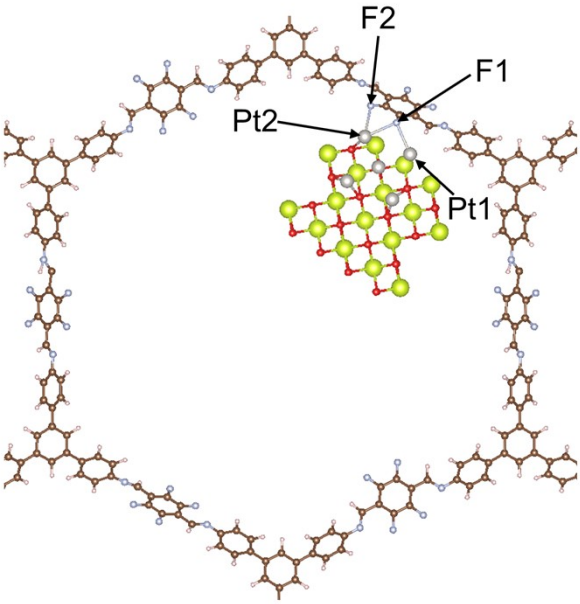

Atom	Pt1	Pt2	F1	F2
Bader (e)	-0.133	0.03	0.63	0.61

Fig. S14 An optimized structural model of CeO_2@Pt@TAFA (top), and calculated Bader charges (bottom).

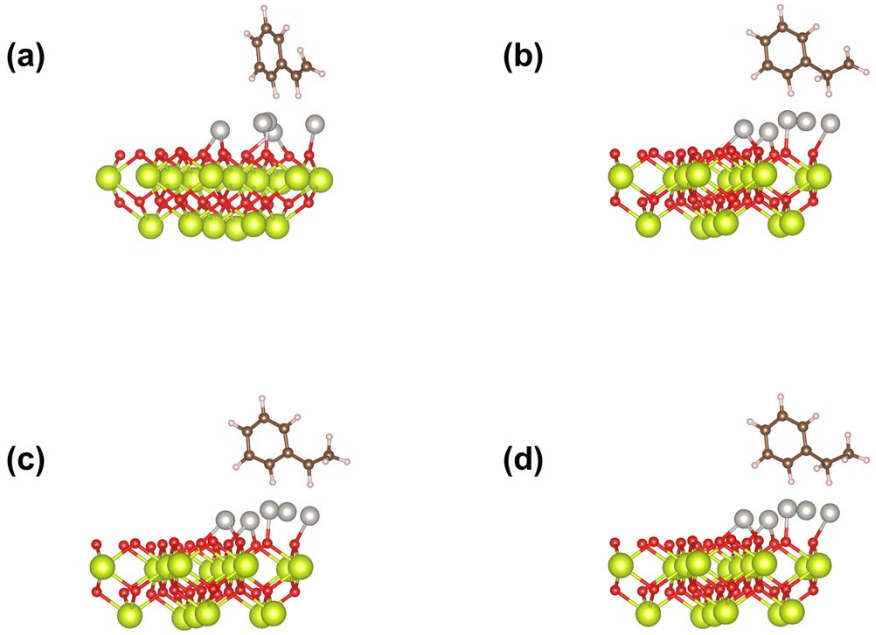

Fig. S15 Structure of the hydrogenation pathway of styrene in CeO_2@Pt@ system.

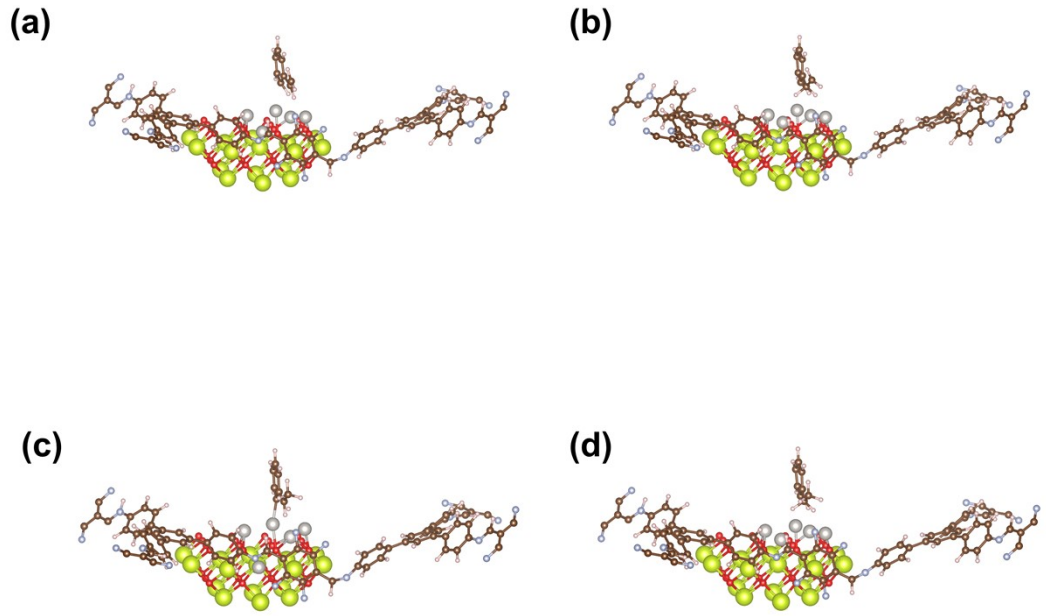

Fig. S16 Structure of the hydrogenation pathway of styrene in CeO_2@Pt@TAFA system.

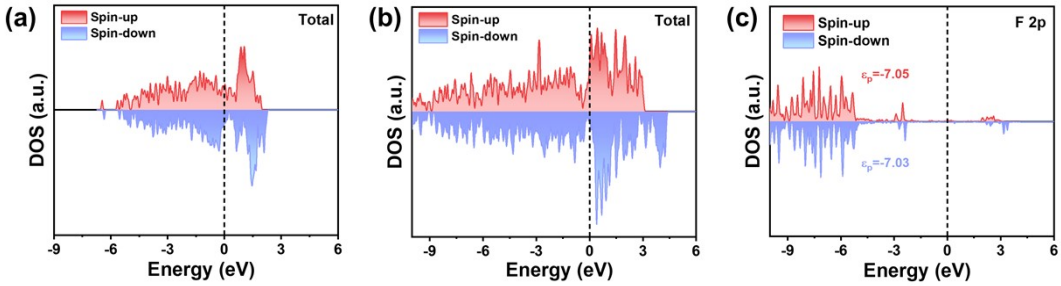

Fig. S17 Total Density of states (DOS) of (a) CeO_2@Pt and (b) CeO_2@Pt@TAFA. (c) DOS of F in CeO_2@Pt@TAFA.

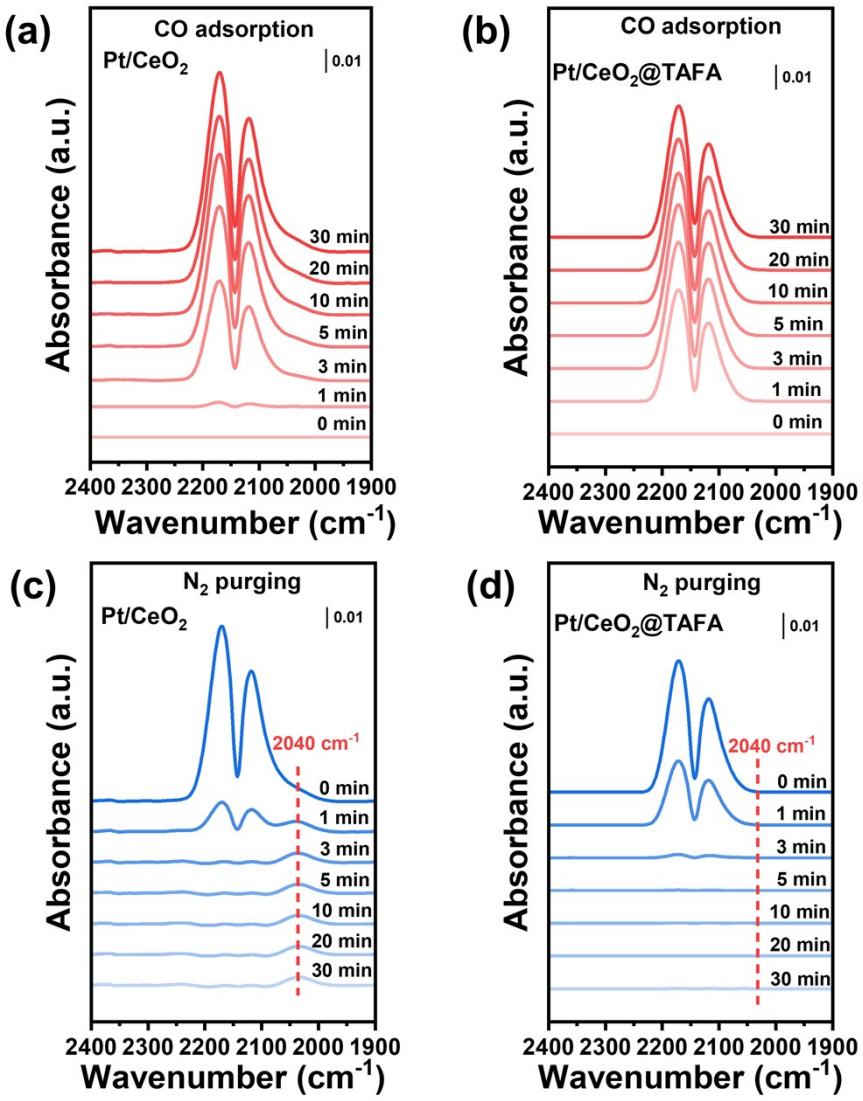

Fig. S18 Schematic illustration of two possible reaction pathways for the hydrogenation process of CO.

CO adsorption experiments provided further evidence for the electronic and spatial modulations introduced by the TAFA shell. Specifically, in situ DRIFTS analysis revealed characteristic bands associated with linear CO adsorption on metallic Pt^0 centers (**Figs. S18a, b**). Upon N_2 purging, a weak shoulder at ~2040 cm^{-1}, corresponding to bridged CO species (Pt–CO–Pt), appeared in CeO_2@Pt (**Fig. S18c**), indicating the presence of contiguous, electron-rich Pt ensembles. In contrast, this

bridged CO band was absent in CeO_2@Pt@TAFA (**Fig. S18d**), suggesting significant alterations in both the electronic structure and spatial configuration of Pt sites. This change likely results from (i) reduced Pt–Pt proximity due to steric confinement within the TAFA shell, and (ii) electron depletion at Pt centers induced by the electron-withdrawing fluorinated matrix, which suppresses multi-site adsorption. These findings are supported by DFT-derived Bader charge analysis and d-band center shifts, confirming the formation of electron-deficient $Pt^{\delta+}$ species. Altogether, the elimination of bridged CO adsorption highlights the dual-interface modulation, via electronic tuning and spatial isolation, as a key factor in achieving superior aqueous-phase hydrogenation performance.

Table 1 BET data statistics

Entry	Samples	Pt loading（wt %）	BET surface area（$m^2 \cdot g^{-1}$）	V_t（$cm^3 \cdot g^{-1}$）	d_{BJH}（nm）
1	CeO_2@Pt	0.98	120.31	0.28	8.49
2	CeO_2@Pt-PB	0.87	127.47	0.32	9.17
3	CeO_2@Pt@TPA	0.76	124.7	0.21	8.33
4	CeO_2@Pt@TAFA	0.73	137.63	0.23	8.21

References

[1] Kresse, G.; Hafner, J. Ab Initio Molecular Dynamics for OpenShell Transition Metals. Phys. Rev. B 1993, 48 (17), 13115−13118.

[2] Kresse, G.; Hafner, J. Ab Initio Molecular Dynamics for Liquid Metals. Phys. Rev. B 1993, 47 (1), 558−561.

[3] Perdew, J. P.; Burke, K.; Ernzerhof, M. Generalized Gradient Approximation Made Simple. Phys. Rev. Lett. 1996, 77 (18), 3865−3868.

[4] Kresse, G.; Joubert, D. From Ultrasoft Pseudopotentials to the Projector Augmented-Wave Method. Phys. Rev. B 1999, 59 (3), 1758−1775.

[5] Grimme, S.; Antony, J.; Ehrlich, S.; Krieg, H. A Consistent and Accurate Ab Initio Parametrization of Density Functional Dispersion Correction (DFT-D) for the 94 Elements H-Pu. J. Chem. Phys. 2010, 132 (15), 154104.